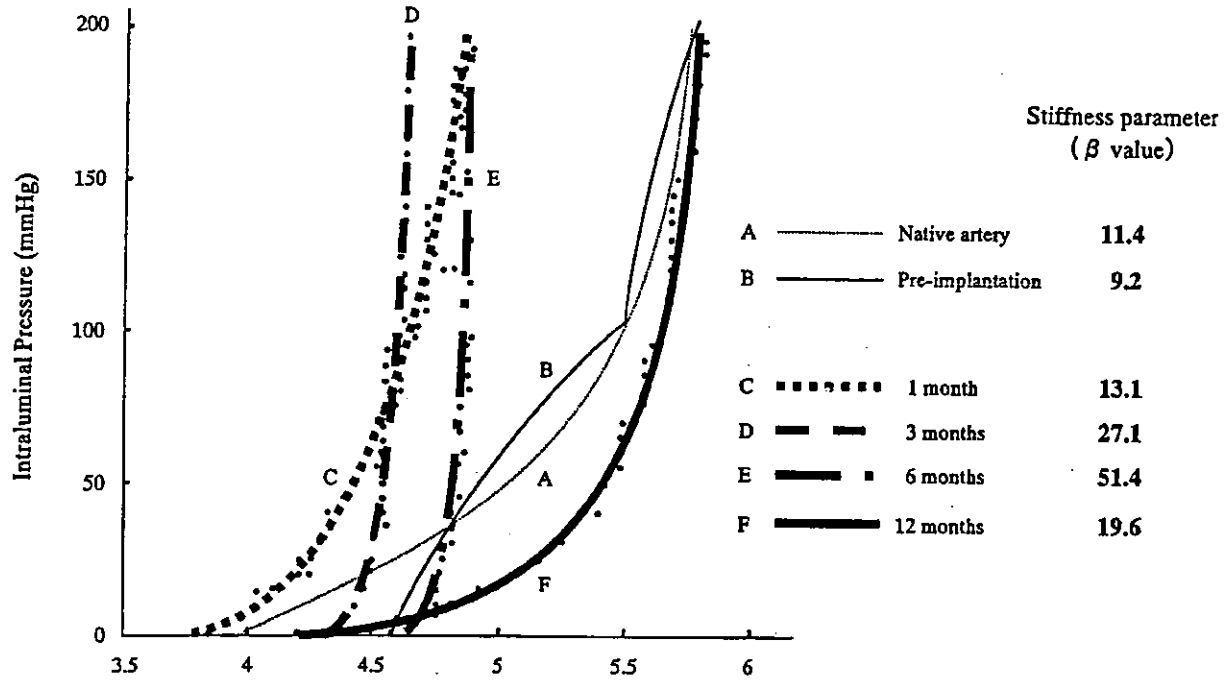

Figure 12. Time-dependent changes of the pressure-diameter relationship of the grafts and the stiffness parameters (β values) after implantation.

photoreactive gelatin mixed with heparin for the inner tube and photoreactive hydrophilic polymer for the outer tube. The photografting of these substances on respective tubes by UV light irradiation resulted in the formation of covalently bonded graft layers.

Although the patency rate was comparably high (~86%), thrombus formation was partially observed on the luminal surface of the graft at 1 and 3 months after implantation. This result indicated that although the heparin immobilized in and released from the photoreactive gelatin layer appears to help suppress thrombus formation, its loading amount appears to be insufficient for preventing thrombus formation. The luminal surface was completely endothelialized at 6 months after implantation. On the other hand, the outer tube photografted with the nonionically hydrophilic polymer eventually prevented the adhesion between the surface and the ingrown tissues. However, the neoarterial tissue, which regenerated in the interspace between the outer and inner tubes through the micropores of the outer tube, adhered to the outer surface of the inner tube. In addition, foreign body reactions such as encapsulation or fibrosis occurred at the outer surface of the outer tube. These combined effects appear to be responsible for the stiffening of the implanted graft with increasing implantation period (Fig. 12). The major components of the neoarterial tissue were myofibroblasts and inflammatory cells in the early phase, and collagen-rich extracellular matrices were produced with time. This appears to be the normal wound healing process. However, although well-aligned SMC layers beneath the intima were observed, the elastic fibers were not produced even at 12 months after implantation.

Increased stiffening of the implanted grafts and impaired J curve were noted with time, probably because of the regenerated neoarterial wall and tissue adhesion to the inner tube, as described above. On the other hand, the revert-back J curve observed at 12 months after implantation was closely associated with the deterioration of SPU, which was evidenced by crack development at laser-ablated micropores and its radial propagation, resulting in the deterioration of mechanical properties. In fact, the mechanical strength of the micropored SPU films retrieved at 12 months after implantation decreased approximately to one-tenth of that of the preimplanted SPU films (data not shown). This may be due to stress concentration at the edge of micropores caused by continuously loaded pulsatile stress as well as material deterioration derived from high-energy pulsed laser ablation at the edge. This material deterioration was not expected because segmented polyurethane, Cardiomat 610, has a well-proven decrability when it has been used for fabrication of commercial blood pumps such as intra-aortic blood pump and left ventricular device. However, the structural and concomitant mechanical deterioration observed in this study may imply that biodegradation rate is much faster in tissues than in circulating blood and that stress-concentration generated during fabrication enhances biodegradation.

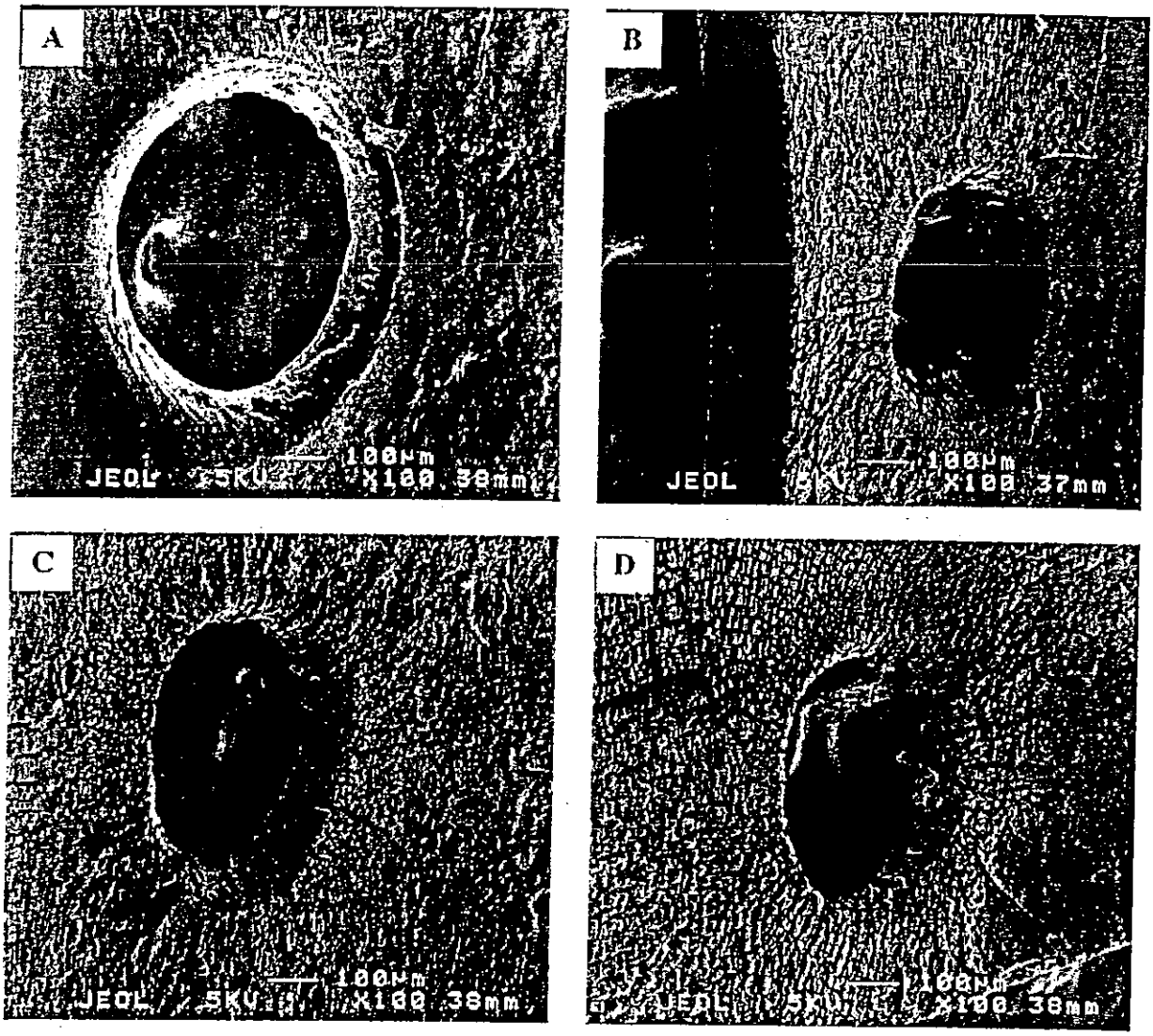

Figure 13. Scanning electron microscopic findings of the surface of the segmented polyurethane films before and after implantation. (A) At preimplantation. (B) At 3 months after implantation. (C) At 6 months after implantation. (D) At 12 months after implantation. Original magnification, ×100.

These two effects appear to synergistically operate in this particular application. Therefore, a more durable segmented polyurethane using polycarbonate as a soft segment must be used for fabrication of coaxial double-tubular artificial grafts.

The concept and fabrication of coaxial double-tubular compliant grafts composed of very thin multiply micropored SPU films are quite unique; these were designed and constructed from biomechanical and biomaterial viewpoints. The J curve in the P-D relationship was realized in the early stage of implantation. However, the occurrence of an impaired P-D relationship with increasing implantation period indicates that manipulation of tissue ingrowth and strict prevention of tissue adhesion are essential for this system. The key issues to be resolved in future study are surface processing technology leading to more precise control of tissue ingrowth including encapsulation and tissue adhesion prevention, and material design for producing highly durable SPU. Once these are materialized, this uniquely structured artificial graft will function well to exhibit biomechanically functional adaptation and controlled tissue architecture.

References

1. Kinley CE, Marble AE. Compliance: a continuing problem with vascular grafts. J Cardiovasc Surg 1980;21:163–170.
2. Burton AC. Relation of structure to function of the tissues of the wall of blood vessels. Physiol Rev 1954;34:619–642.

3. Friedman SG, Lazzaro RS, Spier LN, Moccio C, Tortolani AJ. A prospective randomized comparison of Dacron and polytetrafluoroethylene aortic bifurcation grafts. Surgery 1995;117:7–10.
4. Prager M, Polterauer P, Bohmig HJ, Wagner O, Fugl A, Kretschmer G, Plohner M, Nanobashvili J, Huk I. Collagen versus gelatin-coated Dacron versus stretch polytetrafluoroethylene in abdominal aortic bifurcation graft surgery: results of a seven-year prospective, randomized multicenter trial. Surgery 2001;130:408–414.
5. Pevec WC, Darling RC, L'Italien GJ, Abbott WM. Femoropopliteal reconstruction with knitted, nonvelour Dacron versus expanded polytetrafluoroethylene. J Vasc Surg 1992;16:60–65.
6. Devine C, Hons B, McCollum C. Heparin-bonded Dacron or polytetrafluoroethylene for femoropopliteal bypass grafting: a multicenter trial. J Vasc Surg 2001;33:533–539.
7. Abbott WM, Megerman J, Hasson JE, L'Italien G, Warnock DF. Effect of compliance mismatch on vascular graft patency. J Vasc Surg 1987;5:376–382.
8. Kidson IG, Abbott WM. Low compliance and arterial graft occlusion. Circulation 1978;58(Suppl):I1–I4.
9. Qiu Y, Tarbell JM. Computational simulation of flow in the end-to-end anastomosis of a rigid graft and a compliant artery. ASAIO J 1996;42:M702–M709.
10. Stewart SF, Lyman DJ. Effects of a vascular graft/natural artery compliance mismatch on pulsatile flow. J Biomech 1992; 25:297–310.
11. Sonoda H, Takamizawa K, Nakayama Y, Yasui H, Matsuda T. Small-diameter compliant arterial graft prosthesis: Design concept of coaxial double tubular graft and its fabrication. J Biomed Mater Res 2001;55:266–276.
12. Nakayama Y, Ishibashi K, Matsuda T. Benzophenone-derivatized gelatin as photocurable hemostatic glue: Gelation characteristics by an excimer laser irradiation and its in vivo performance. Jpn J Artif Organs 1995;24:102–105.
13. Doi K, Nakayama Y, Matsuda T. Novel compliant and tissue-permeable microporous polyurethane vascular prosthesis fabricated using an excimer laser ablation technique. J Biomed Mater Res 1996;31:27–33.
14. Doi K, Matsuda T. Enhanced vascularization in a microporous polyurethane graft impregnated with basic fibroblast growth factor and heparin. J Biomed Mater Res 1997;34:361–370.
15. Doi K, Matsuda T. Significance of porosity and compliance of microporous, polyurethane-based microarterial vessel on neoarterial wall regeneration. J Biomed Mater Res 1997;37:573–584.
16. Matsuda T, Inoue K, Sugawara T. Development of micropatterning technology for cultured cells. ASAIO Trans 1990;36: M559–62.
17. Sonoda H, Urayama S, Takamizawa K, Nakayama Y, Uyama C, Yasui H, Matsuda T. Compliant design of artificial graft: compliance determination by new digital X-ray imaging system-based method. J Biomed Mater Res 2002;60:191–195.
18. Hayashi K, Nakamura T. Material test system for the evaluation of mechanical properties of biomaterials. J Biomed Mater Res 1985;19:133–144.
19. Hayashi K, Handa H, Nagasawa S, Okumura A, Moritake K. Stiffness and elastic behavior of human intracranial and extracranial arteries. J Biomech 1980;13:175–184.
20. van der Lei B, Nieuwenhuis P, Molenaar I, Wildevuur CR. Long-term biologic fate of neoarteries regenerated in microporous, compliant, biodegradable, small-caliber vascular grafts in rats. Surgery 1987;101:459–467.
21. Okoshi T, Soldani G, Goddard M, Galletti PM. Penetrating micropores increase patency and achieve extensive endothelialization in small diameter polymer skin coated vascular grafts. ASAIO J 1996;42:M398–401.
22. Hsu S, Kambic H. On matching compliance between canine carotid arteries and polyurethane grafts. Artif Organs 1997;21: 1247–1254.

In vivo leukocyte cytokine mRNA responses to biomaterials are dependent on surface chemistry

William G. Brodbeck,[1] Gabriela Voskerician,[2] Nicholas P. Ziats,[1,2] Yasuhide Nakayama,[3] Takehisa Matsuda,[4] James M. Anderson[1,2]
[1]*Department of Pathology, Case Western Reserve University, Cleveland, Ohio 44106*
[2]*Department of Biomedical Engineering, Case Western Reserve University, Cleveland, Ohio 44106*
[3]*Department of Bioengineering, National Cardiovascular Center, Osaka, Japan*
[4]*Department of Biomedical Engineering, Kyushu University, Fukuoka, Japan*

Received 8 March 2002; revised 13 May 2002; accepted 16 May 2002

Abstract: An *in vivo* mouse cage implant system was used to determine whether leukocyte cytokine mRNA responses to implanted biomaterials were dependent on surface chemistry. Surfaces displaying various chemistries (hydrophobic, hydrophilic, anionic, and cationic) were placed into stainless steel cages and implanted subcutaneously. Semiquantitative RT-PCR analyses revealed that hydrophilic surfaces showed a decreased expression of proinflammatory cytokines, IL-6 and IL-8, and pro-wound healing cytokines, IL-10 and TGF-β by adherent cells, and mRNA levels of the proinflammatory cytokine, IL-1β, and the pro-wound healing cytokine IL-13 were decreased in surrounding, exudate cells. Cytokine responses by adherent and exudate cells to hydrophobic, anionic and cationic surfaces were similar and indicative of a strong inflammatory response at the earliest time point followed by a wound healing response at later time points. However, no differences in the types or levels of exudate cells for any of the surfaces or the empty cage at each of the respective time points were observed, indicating their respective biocompatibility. These studies identify hydrophilic surface chemistries as having significant effects on leukocyte cytokine responses *in vivo* by decreasing the expression of inflammatory and wound healing cytokines by inflammatory cells adherent to the biomaterial as well as present in the surrounding exudate. © 2002 Wiley Periodicals, Inc. J Biomed Mater Res 64A: 320–329, 2003

Key words: biocompatibility; cytokines; inflammation; leukocytes; wound healing

INTRODUCTION

After implantation of biomedical devices and prostheses, the surface of the implanted material is immediately coated with plasma proteins followed by adhesion of leukocytes of the myeloid lineage (namely neutrophils and blood-derived monocytes) that recognize and bind to the adsorbed proteins through cell surface integrin receptors.[1] Adherent monocytes differentiate into macrophages which fuse to form multinucleated foreign body giant cells (FBGCs).[2–6] FBGCs are adherent to the surface of the implant for its *in vivo* lifetime[7] and act to concentrate macrophage phagocytic and degradative activities that result in oxidative damage and stress cracking of the implanted material.[8,9] Additionally, adherent monocytes/macrophages secrete cytokines in response to the implant that direct the recruitment of more leukocytes (of both the myeloid and lymphoid lineages) and other cell types, including fibroblasts, to the tissue/material interface. The nonadherent cells present within the exudate fluid surrounding the implant (such as neutrophils, monocytes, and lymphocytes) also secrete cytokines that direct leukocyte chemotaxis and activation as well as the activities of the biomaterial adherent leukocyte population. Thus, cytokines secreted by biomaterial adherent and surrounding exudate leukocytes can direct the overall response to the implanted biomedical device and prosthesis.

Cytokines are traditionally categorized as Th1 and Th2 types, referring to the patterns secreted by subpopulations of CD4+ T cells that determine the outcome of an antigenic response, being toward either a cellular or humeral driven response, respectively. A number of other cell types, other than CD4+ cells, produce Th1 and Th2 cytokines, including macrophages and neutrophils.

Correspondence to: J. M. Anderson; e-mail: wgb2@po.cwru.edu

Contract grant sponsor: National Institutes of Health; contract grant numbers: GM-20380 (fellowship awarded to W.G.B.), HL-33849, HL-55714

In terms of biomaterial biocompatibility, cytokines are described based on their role in influencing the foreign body response to the implanted material. The sequence of events directed by cytokines that progresses after implantation of a biomaterial is acute inflammation, which leads into chronic inflammation. As inflammation resolves, the wound healing response progresses resulting in the formation of an avascular fibrous capsule surrounding the implant (reviewed in Ref. 10). Therefore, when describing the foreign body response to implanted materials, cytokines are classified as being either proinflammatory or pro-wound healing, depending on which events they promote (Fig. 1). Interleukin-2 (IL-2), interleukin-6 (IL-6), interleukin-8 (IL-8), and tumor necrosis factor alpha (TNF-α) are considered proinflammatory/anti-wound healing cytokines because of their collective ability to promote inflammation by cellular activation and chemotaxis. Cytokines that inhibit the inflammatory response and promote wound healing, such as interleukin-1 receptor antagonist (IL-1RA), interleukin-4 (IL-4), interleukin-13 (IL-13), and transforming growth factor beta (TGF-β), are considered anti-inflammatory/pro-wound healing. Interleukin-1 beta (IL-1β and interleukin-10 (IL-10) are two unique cytokines in this classification scheme because they represent the extremes of the responses. IL-1β is considered a proinflammatory/pro-wound healing cytokine because of its ability to activate both inflammatory cells (lymphocytes and monocytes) and wound healing cells (fibroblasts). IL-10 acts in the opposite fashion by downregulating the activity of these cell types and suppressing further cytokine production, leading to an anti-inflammatory/anti-wound healing effect.

In addition to deciding the fate of implanted devices or prostheses by guiding the foreign body response, cytokines present in the local milieu dictate macrophage superoxide generation and fusion into FBGCs,[11–13] contributing to the failure of the implant. Therefore, it is essential to identify mechanisms that control the types and levels of cytokines produced by adherent and exudate leukocytes to engineer biomaterials that provide implants that are more acceptable to the body.

A promising method of controlling biological responses to biomaterial implants is through surface modification of implantable materials. To investigate this potential mechanism, polyethylene terephthalate (PET) surfaces were modified by photograft copolymerization to yield hydrophobic, hydrophilic, anionic, and cationic chemistries, which model materials that are currently used and candidate materials in medical devices and prostheses. Surfaces were placed within stainless steel wire mesh cages and implanted subcutaneously into Balb/C mice. At days 7, 14, and 21, exudates surrounding the surfaces within the cages were drawn and surfaces explanted. Adherent and exudate leukocytes were lysed and total RNA extracted, reversibly transcribed and polymerase chain reaction (PCR) amplified to test adherent IL-1β, TNF-α, IL-6, IL-8, IL-1RA, IL-10, and TFG-β and exudate IL-1β, IL-6, IL-2, IL-8, IL-10, IL-4, and IL-13 mRNA expression levels. In other samples, exudate cells were analyzed for total and differential cell counting while adherent cells were stained to determine leukocyte adhesion and macrophage fusion rates to form FBGCs. These are the first studies to describe a biomaterial surface chemistry as having an influence on adherent and exudate leukocyte cytokine production. This information is necessary to further guide the development of biomedical devices and prostheses to initiate/inhibit desired leukocyte/cytokine responses.

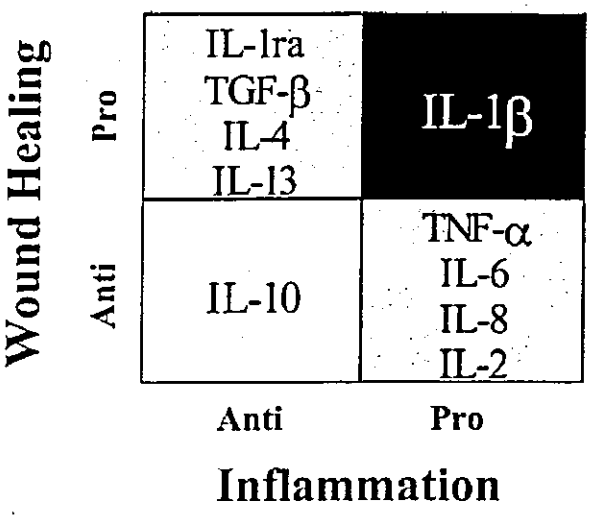

Figure 1. Classification of cytokines. Gantt chart representing the classification of cytokines according to their roles in the foreign body response.

MATERIALS AND METHODS

Preparation of surfaces

Biomaterial surfaces displaying distinct surface chemistries were prepared with a custom-designed, semiautomatic apparatus for laboratory-scale mass production as previously described.[14,15] The base surface consisted of polyethylene terephthalate (PET) film. Modification followed by first coating the PET film with poly (benzyl *N,N*-diethyldithiocarbamate-*co*-styrene) (BDEDTC). Either polyacrylamide (PAAm), sodium salt of poly(acrylic acid) (PAANa), or methiodide of poly(dimethylaminopropyl-acrylamide) (DMAPAAmMeI) were photograft copolymerized to the BDEDTC surface. This provided slightly hydrophobic (PET), hydrophobic (BDEDTC), hydrophilic (PAAm), anionic (PAANa), and cationic (DMAPAAmMeI)

surfaces, respectively, as previously characterized and described.[16]

Mouse cage implant system

Implants were performed as previously described.[17-21] Briefly, surfaces were placed in surgical-grade stainless steel wire mesh cages (1.5 cm in length, 0.5 cm in diameter, 0.25 mm wire diameter, 0.8 mm opening width with 58% open area) and sterilized with ethylene oxide. Cages containing surfaces were implanted subcutaneously in the backs at the level of the panniculus carnosus of anesthetized, 8-week-old 50- to 70-g female Balb/C mice (Jackson, Bar Harbor, ME). IACUC and NIH guidelines for the care and use of laboratory animals were observed.

At days 7, 14, and 21 after implantation, exudate fluid contained within the cages, surrounding the implants were drawn and surfaces explanted. Exudates were split into two groups and processed as described below. Adherent cells were either stained for light microscopic observations or processed for total RNA isolation as described below.

Adhesion and fusion analyses

On days 7, 14, and 21 after implantation, adherent cell densities and macrophage fusion were determined after staining by May Grünwald/Giemsa. Surfaces were rinsed with PBS twice, and adherent cells were fixed by the addition of methanol for 5 min. Cells were washed with PBS, and May Grünwald reagent was added for 1 min. After another PBS wash, Giemsa reagent, was added for 5 min, and samples were rinsed by a final wash with dH_2O. Cell densities were determined from five 200× fields for each sample and are expressed as cells per mm^2. Nuclei contained within multinucleated foreign body giant cells were each counted as individual cells for determination of cell densities. Percent fusion was calculated by dividing the number of nuclei contained within giant cells by total number of nuclei in the field of view. This was repeated for three 200× fields.

Exudate analyses

On days 7, 14, and 21, 100–500 μL of exudate surrounding the implant within the cages were drawn prior to explantation. One half of the exudate was processed for total leukocyte and differential cell counting (described in Ref. 21). The other half of the exudate was centrifuged, pelleted cells rinsed twice in PBS and total RNA extracted by TRIZOL, as described below.

Semiquantitative RT-PCR

To quantitatively assess cellular expression levels of cytokines, total RNA was isolated from adherent and exudate cells at the indicated time points using TRIZOL Reagent (Gibco BRL, Gaithersburg, MD) according to the manufacturer's instructions. For adherent cells, surfaces were rinsed twice with PBS solution, and 250 μL of TRIZOL were added to each well. Duplicate samples were combined to ensure sufficient amounts of RNA, yielding 500 μL of cell extract per surface per condition. For exudate cells, cells were washed twice with PBS followed by the addition of 500 μL TRIZOL. For either cell population, the extract was allowed to stand for 10 min and centrifuged at 10K rpm for 10 min. The pellets were discarded, and supernatants containing RNA were then mixed with 100 μL chloroform and inverted repeatedly for 15 s followed by 3-min incubation and centrifugation for 15 min at 10K rpm. The resulting aqueous layer was then combined with 300 μL of isopropanol and mixed thoroughly. RNA was then pelleted and washed with 75% ethanol in autoclaved water. Eleven microliters of autoclaved water were used to dissolve the RNA by incubating at 55°C for 10 min.

Messenger RNA was reversibly transcribed by combining the samples with 1 μL oligo$(dT)_{12-18}$ primer (Gibco-BRL) and incubating for 10 min at 70°C. A mixture of 4 μL 5× first strand buffer, 2 μL 0.1*M* DTT, and 1 μL of 10 m*M* dNTP mix was then added to the sample and incubated for 2 min at 42°C. Reverse transcription was then initiated by the addition of 1 μL (200 units) Superscript II (Gibco-BRL Life Technologies), and the reaction was incubated at 42°C. After 50 min, the reaction was inactivated by heating the mixture to 70°C for 15 min. The reversibly transcribed product was then stored at −70°C or immediately used for PCR amplification.

PCR was performed using a GeneAMP 9700 PCR System (PE Applied Biosciences). Five microliters of reversibly transcribed product were mixed with 10 μL 10× PCR buffer, 3 μL 50 m*M* $MgCl_2$, 2 μL 10 m*M* dNTP mix, and 1 μL Taq DNA polymerase (5 U/μL; Gibco-BRL Life Technologies) were used per reaction tube. Autoclaved water was then used to bring each reaction volume to 100 μL. Primer pairs were added to a final concentration of 10 μ*M*. The primer pairs used to amplify specific cytokine and β-actin sequences are listed in Table I. The amplification was then performed for 35 cycles (94°C for 30 s, 60°C for 30 s, and 72°C for 30 s per cycle).

The resulting amplified products were separated by electrophoresis through 1.5% agarose and visualized by UV of the intercalated ethidium bromide. Photographs were then digitally scanned, and using SigmaScanPro 4.0 the band intensities were quantified. Expression ratios were determined by dividing the band intensity of the product of interest by that of the corresponding β-actin band. The intensity of this standard "housekeeping" gene (β-actin) varies with cell number and cell activation state. Therefore, by comparing the intensity of the product of interest to that of β-actin isolated from the same sample, variations among cell densities and activation states are normalized.

Statistical analyses

Data are expressed as the average of replicate experiments utilizing cells from three different animals ± the standard

TABLE I
Cytokine Specific Mouse Primers

Amplified RNA	Primer Sequences (5'–3')	Reference
β-Actin	Sense: GTGGGCCGCTCTAGGCACCAA Antisense: CTCTTTGATGTCACCACGATTTC	25
IL-1β	Sense: ATGGCAACTGTTCCTGAACTCAACT Antisense: CAGGACAGGTATAGATTCTTTCCTTT	25
IL-1RA	Sense: GGCAGCCTGCCGCCCTTCTGGG Antisense: CTCAAAGCTGGTGGTGGGGCC	26
IL-2	Sense: TTCAAGCTCCACTTCAAGCTCTACAGCGGA Antisense: GACAGAAGGCTATCCATCTCCTCAGAAGCC	25
IL-4	Sense: TCTTTCTCGAATGTACCAGG Antisense: CATGGTGGCTCAGTACTACG	25
IL-6	Sense: TGCTGGTGACAACAACGGCC Antisense: GTACTCCAGAAGACCAGAGG	25
IL-8	Sense: TTGGCAGCCTTCCTGATTTC Antisense: AACTTCTCCACAACCCTCCTG	27
IL-10	Sense: ATGCAGGACTTTAAGGGTTACTTGGGTT Antisense: ATTCGGAGAGAGAGGTACAAACGAGGTTT	25
IL-13	Sense: GCCAGCCCACAGTTCTACAGC Antisense: GTGATGTTGCTCAGCTCCTCA	28
TGF-β	Sense: GAAGCCATCCGTGGCCAGAT Antisense: GACGTCAAAAGACAGCCACT	25
TNF-α	Sense: TTGACCTCAGCGCTGAGTTG Antisense: CCTGTAGCCCACGTCGTAGC	25

error of the mean. Statistical comparisons were performed using the Student's unpaired *t* tests, using StatView v4.1 (Abacus Concepts, Berkeley, CA).

RESULTS

Biomaterial adherent leukocyte cytokine expression is shown in Figure 2. On day 7 after implantation [Fig. 2(A)], leukocytes adherent to hydrophobic surfaces expressed significantly decreased levels of IL-6 and IL-8 ($p < 0.05$) when compared with the PET base surface, whereas hydrophilic surface leukocytes expressed significantly decreased levels of IL-6, IL-8, IL-10, and TGF-β ($p \leq 0.02$). By day 14 after implantation, no significant differences were observed in the expression levels of adherent cells for all cytokines tested except for a decrease in IL-8 and TGF-β mRNA within hydrophilic surface adherent leukocytes [Fig. 2(B)]. This decrease remained consistent by implant day 21, along with a significant decrease in IL-β, IL-6, and IL-10 expression in cells adherent to the hydrophilic surface [Fig. 2(C)].

Adherent leukocyte cytokine levels were independent of the rate of leukocyte adhesion and macrophage fusion to form foreign body giant cells (Fig. 3). As shown in Figure 3(A), on day 7 of implantation, hydrophobic and cationic surfaces provided signifi-

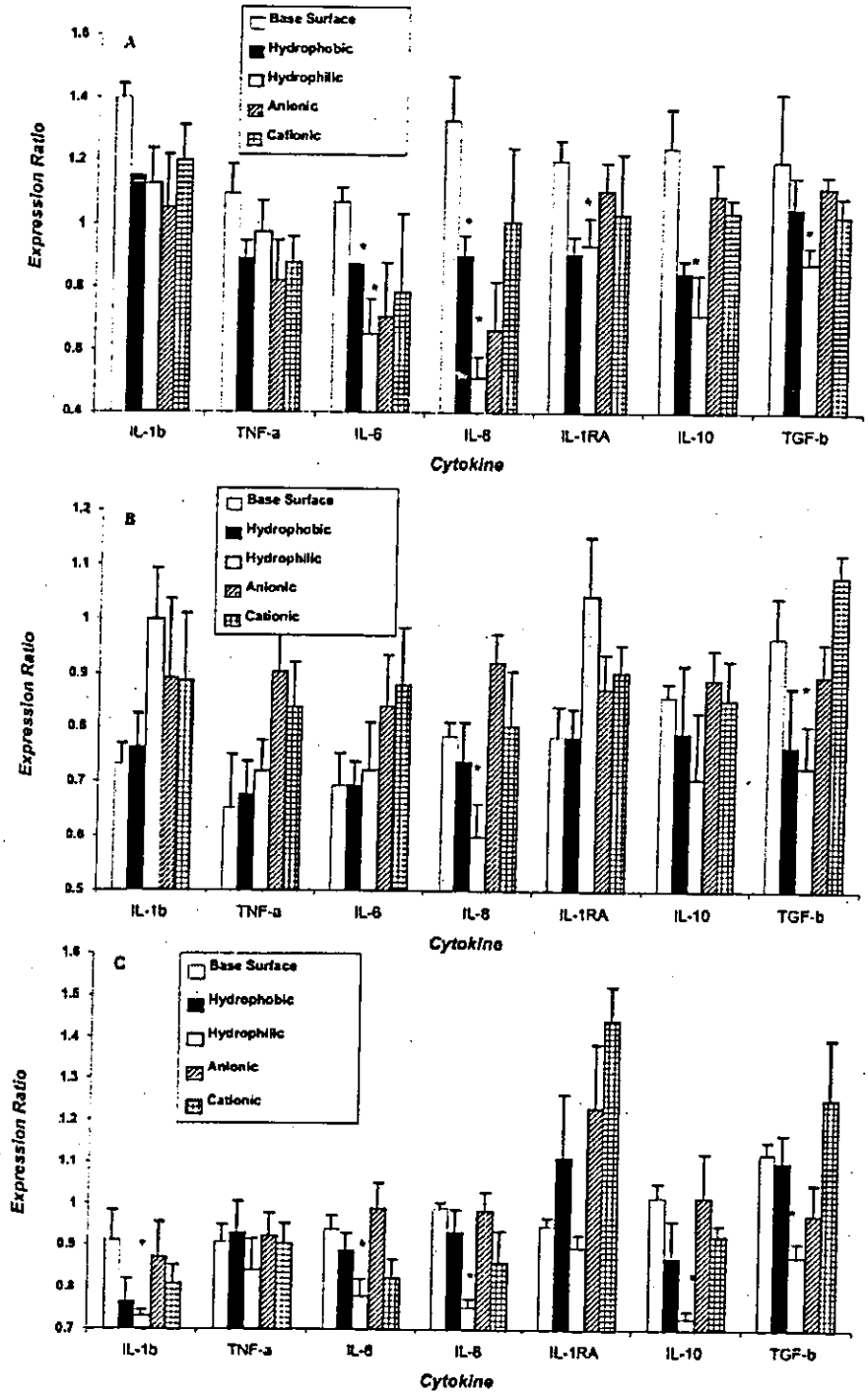

Figure 2. Biomaterial adherent cell cytokine expression. Total RNA from cells adherent to biomaterials was isolated on days 7 (A), 14 (B), and 21 (C) after implantation. Messenger RNA was reversibly transcribed and corresponding cytokine and β-actin transcripts were amplified by PCR. Messenger RNA was reversibly transcribed and corresponding cytokine or β-actin mRNAs PCR amplified. Data are shown as expression ratios and are a result of the mean of three animals ± the standard error of the mean. *Significantly reduced levels of expression ($p < 0.05$) when compared with the PET base surface. Note different expression ratio (y axis) scale for each time point.

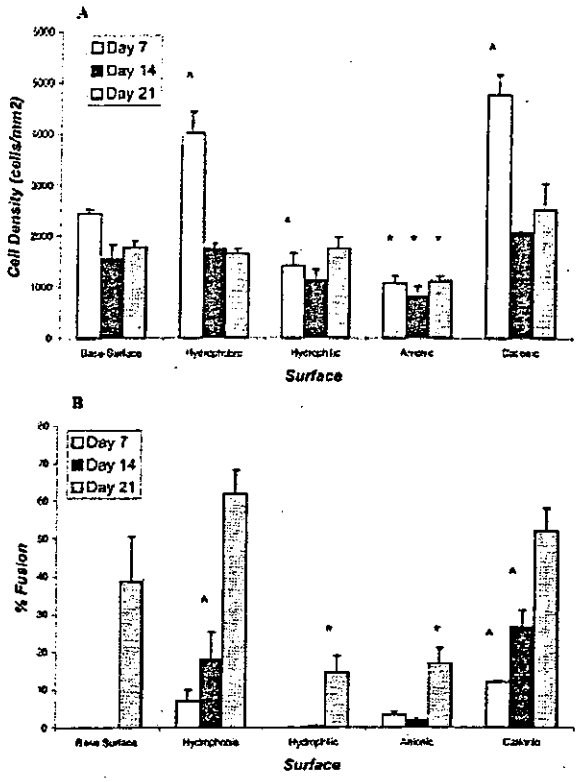

Figure 3. Leukocyte adhesion and macrophage fusion on implanted biomaterials. Surfaces were explanted on days 7, 14, and 21 and washed with PBS. Adherent cells were stained with May-Grünwald/Giemsa for determination of cell adhesion (A) and macrophage fusion (B). Results are expressed as the mean of three implants taken from separate mice ± the standard error of the mean. *Significantly decreased values; ^ significantly increased values when compared with the PET base surface ($p < 0.05$).

cantly increased levels of leukocyte adhesion (4020 ± 419 and 4770 ± 225 cells/mm^2, respectively) above base surface levels (2440 ± 84 cells/mm^2, $p \leq 0.032$), whereas hydrophilic surfaces promoted decreased levels of leukocyte adhesion (1420 ± 252 cells/mm^2, $p = 0.0183$). Significantly decreased leukocyte adhesion rates were present on anionic surfaces at all time points tested when compared with all surfaces tested. Rates of macrophage fusion to form FBGCs were significantly increased on hydrophobic surfaces at day 7 (7 ± 2.9%) and on cationic surfaces on days 7 and 14 (12 ± 0.33 and 26.7 ± 4.4%) [Fig. 3(B)] when compared with the base surface. Conversely, fusion rates were significantly lower on hydrophilic and anionic surfaces on day 21 (4.5 ± 4.5 and 17 ± 4%, respectively, $p < 0.0257$, when compared with PET fusion rates).

Cytokine expression ratios for exudate cells are shown in Figure 4. On day 7 after implantation, cells surrounding the anionic surfaces expressed significantly lower levels of IL-8 [Fig. 4(A)], whereas hydrophilic surface exudate cells expressed lower levels of IL-13, which was apparent through days 14 and 21 [Fig. 4(B,C)] $p \leq 0.023$ when compared with PET expression levels). Exudate cells surrounding the hydrophilic surfaces also expressed significantly lower levels of IL-1β on days 14 and 21 and lower levels of IL-6 and IL-2 by day 21 ($p \leq 0.031$ when compared with the base surface exudate cells). Hydrophobic and cationic surfaces promoted significantly increased expression levels of IL-13 on day 21 ($p \leq 0.025$).

Although cytokine expression ratios varied among exudate cells surrounding the different surface chemistries, no significant differences were observed in the total or differential leukocyte counts for any given time point (Table II).

DISCUSSION

The foreign body response to implanted biomedical devices and prostheses is guided by leukocyte-derived cytokines. The types and levels of cytokines surrounding an implanted device may initially drive the acute and chronic inflammatory reactions and later initiate the wound healing response while inflammation resolves. Ideally, implanted devices would forego the foreign body reaction and lead into "normal" wound healing to provide for integration of the implant with the body and not be segregated by an avascular fibrous capsule. Therefore, ways of modulating the foreign body response are currently being sought, and an attractive mechanism is to control the local cytokine production by biomaterial adherent and surrounding exudate leukocytes. These studies were performed to identify potential surface chemistries that significantly influence cytokine production by biomaterial adherent and surrounding, suspended exudate leukocytes.

As summarized in Table III, hydrophilic surfaces caused decreased rates of leukocyte adhesion and macrophage fusion, which confirm our previous *in vitro* and rat *in vivo* studies.[16,22] Also, cytokine production was significantly decreased by cells adherent to this hydrophilic substrate. However, these lowered expression levels were not a direct result from decreased rates of adhesion because decreased adhesion rates were also observed on the anionic surfaces and anionic adherent cells exhibited expression levels similar to those of the base surface. Therefore, we surmise that differential cytokine expression by adherent cells was independent of leukocyte adhesion and macrophage fusion rates.

Adsorption of a biomaterial surface by plasma proteins immediately takes place after introduction to the *in vivo* environment and is the initial step in determining biomaterial biocompatibility. The types, levels, and conformations of proteins adsorbed to the surface (which includes but is not limited to complement pro-

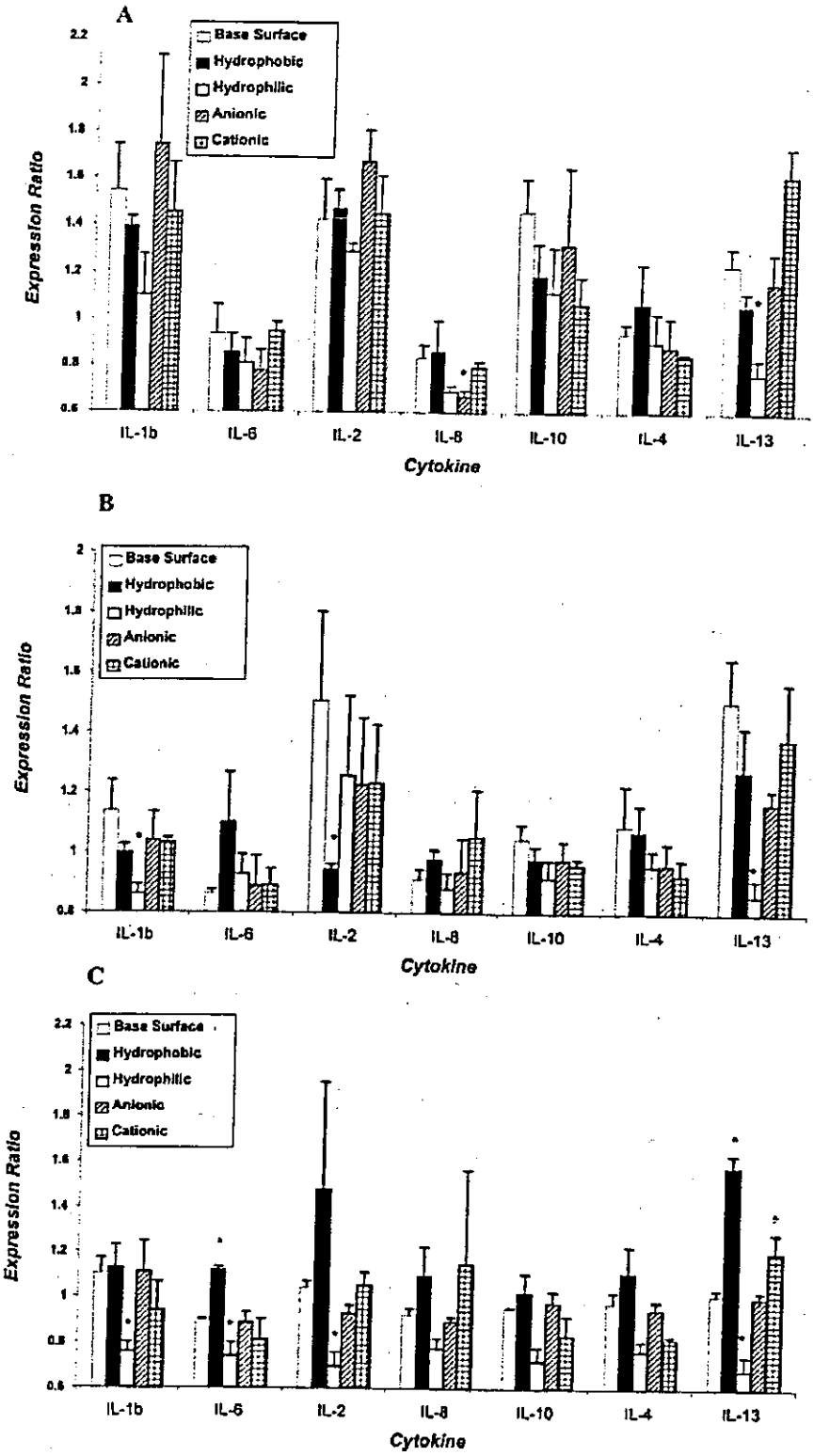

Figure 4. Exudate cell cytokine expression. Total RNA from cells surrounding the biomaterials within the cage was isolated on days 7 (A), 14 (B), and 21 (C) after implantation. Messenger RNA was reversibly transcribed and corresponding cytokine and β-actin transcripts were amplified by PCR. Data are shown as expression ratios and are a result of the mean of three animals ± the standard error of the mean. *Significantly reduced levels of expression ($p < 0.05$) when compared with the PET base surface. Note different expression ratio (y axis) scale for each time point.

TABLE II
Exudate Cell Analysis[a]

Day	Cell Type	Cell Concentration (cells/μl)					
		Empty Cage	Base Surface	Hydrophobic	Hydrophilic	Anionic	Cationic
7	TLC	138 ± 19	133 ± 8	108 ± 8	167 ± 8	167 ± 8	133 ± 8
	Neutrophils	54 ± 9	72 ± 3	57 ± 8	101 ± 36	99 ± 27	64 ± 12
	Monocytes	50 ± 9	65 ± 7	47 ± 7	62 ± 7	64 ± 16	50 ± 11
	Lymphocytes	5 ± 2	6 ± 2	4 ± 1	3 ± 1	3 ± 0	4 ± 0
14	TLC	25 ± 0	33 ± 8	25 ± 0	50 ± 16	33 ± 8	50 ± 16
	Neutrophils	10 ± 0	15 ± 3	5 ± 2	14 ± 4	18 ± 7	16 ± 4
	Monocytes	15 ± 0	19 ± 7	17 ± 0	35 ± 12	15 ± 2	32 ± 12
	Lymphocytes	1 ± 0	1 ± 2	4 ± 1	1 ± 1	1 ± 0	2 ± 0
21	TLC	42 ± 8	33 ± 8	42 ± 17	42 ± 17	50 ± 25	25 ± 0
	Neutrophils	3 ± 1	15 ± 3	3 ± 1	6 ± 2	6 ± 5	7 ± 2
	Monocytes	20 ± 6	19 ± 7	34 ± 14	40 ± 21	36 ± 17	17 ± 2
	Lymphocytes	17 ± 8	1 ± 2	6 ± 4	4 ± 3	8 ± 2	2 ± 1

[a]Data represents the mean of exudates taken from three rats ± the standard error of the mean. TLC, total leukocyte concentration.

teins, fibrinogen, von Willebrand factor, immunoglobulin gamma, fibronectin, and vitronectin) dictate the levels of leukocyte adhesion to that surface and influence the rate of adherent macrophage fusion to form FBGCs.[1] We have previously shown that the chemistry of the biomaterial surface directly influences protein adsorption,[23] and hence, the surface chemistry is also responsible for mediating leukocyte adhesion and macrophage fusion. It is likely that the adsorbed protein layer and subsequent receptor-ligand interactions are responsible for mediating the cytokine responses and partially explain the differential expression patterns observed here and thus support the importance of the initially adsorbed protein layer in determining biomaterial biocompatibility.

Protein adsorption helps determine biocompatibility by indirectly guiding the foreign body response to implanted materials. Three sequential and overlapping stages of this response are acute inflammation, chronic inflammation, and wound healing (reviewed in Reference 10). The general patterns of cytokine expression fit into this sequence. At day 7 after implantation, equally expressed levels of proinflammatory and pro-wound healing cytokines were observed, indicating a strong inflammatory response. By day 14 the levels of proinflammatory cytokine expression decreased, whereas the levels of pro-wound healing cytokine expression remained consistent, favoring a wound healing response at the later time points. The significant exception to this generalized pattern of expression is the hydrophilic surface, which promoted decreased rates of proinflammatory and pro-wound healing cytokines by adherent and exudate cells. The effects of these differential expression patterns on the foreign body response are not known and could not be observed by these experiments. There was no differ-

TABLE III
Relative Adhesion, Fusion, and Cytokine mRNA Expression by Biomaterial Associated Leukocytes[a]

Surface	Day	Adhesion	Fusion	Adherent[b]							Exudate[b]						
				IL-1β	TNF-α	IL-6	IL-8	IL-1RA	IL-10	TGF-β	IL-1β	IL-6	IL-2	IL-8	IL-10	IL-4	IL-13
Hydrophobic	7	↑	—	—	—	↓	↓	↓	↓		—	—	—	—	—	—	—
	14	—	↑	—	—	—	—	—	—	—	—	—	↓	—	—	—	—
	21	—	—	—	—	—	—	—	—	—	—	↑	—	—	—	—	↑
Hydrophilic	7	↓	—	—	—	↓	↓	↓	↓	↓	—	—	—	—	—	—	↓
	14	—	—	—	—	—	↓	—	—	↓	↓	—	—	—	—	—	↓
	21	—	↓	↓	—	↓	↓	—	↓	↓	↓	↓	↓	—	—	↓	↓
Anionic	7	—	—	—	—	—	↓	—	—	—	—	—	—	—	—	—	—
	14	↓	—	—	—	—	—	—	—	—	—	—	—	—	—	—	—
	21	↓	↓	—	—	—	—	—	—	—	—	—	—	—	—	—	—
Cationic	7	↑	↑	—	—	—	—	—	—	—	—	—	—	—	—	—	—
	14	—	↑	—	—	—	—	—	—	—	—	—	—	—	—	—	—
	21	—	—	—	—	—	—	↑	—	—	—	—	—	—	—	↓	↑

[a]—, no significant difference when compared to the PET base surface; ↑, significantly increased value when compared to the base surface; ↓, significantly decreased value when compared to the base surface.
[b]Relative to β-actin expression.

ence in total or differential leukocyte counts when comparing the hydrophilic surface to the base surface or empty cage controls, indicating no effects of leukocyte recruitment or activation. The lack of significantly varying levels of infiltrating leukocytes suggests that all materials are equally biocompatible (according to the established rat cage implant system results).

The pro-wound healing cytokines IL-4 and IL-13 play an integral role in the foreign body response by inducing macrophage fusion to form FBGCs *in vitro*[11–13] and *in vivo*.[24] In the present studies, IL-4 had no differential expression among any surfaces at any time point by exudate leukocytes, whereas IL-13 expression was significantly increased by cells around the hydrophobic and cationic surfaces and significantly reduced in cells surrounding the hydrophilic surface. This is in direct correlation with the increased rates of FBGC formation observed on the hydrophobic and cationic surfaces, indicating that IL-13 mediates fusion of biomaterial adherent macrophages *in vivo* in the mouse model.

It is important to note that we have previously described the ability of the surfaces presented here to dictate rates of macrophage apoptosis *in vitro*[16] and *in vivo*.[22] In those studies we have identified the hydrophilic and anionic surfaces as promoting increased rates of macrophage apoptosis, while not affecting the composition of the surrounding exudate. As described here and elsewhere[16] hydrophilic and anionic surface properties also limit macrophage adhesion and fusion. Furthermore, the studies presented here suggest that hydrophilic surfaces provide a significant inhibition of cytokines secreted by adherent and exudate cells possibly resulting in an attenuated inflammatory reaction. Therefore, hydrophilic surface properties represent an excellent beginning to limiting leukocyte adhesion and activity and influencing the biocompatibility of implanted materials.

References

1. Anderson JM, DeFife KM, McNally AK, Collier TO, Jenney CR. Monocyte, macrophage and foreign body giant cell interactions with molecularly engineered surfaces. J Mater Sci Mater Med 1999;10:579–688.
2. Sutton JS, Weiss L. Transformation of monocytes in tissue culture into macrophages, epithelioid cells, and multinucleated giant cells. J Cell Biol 1966;28:303–332.
3. Murch AR, Grounds MD, Marshall CA, Papadimitriou JM. Direct evidence that inflammatory multinucleated cells form by fusion. J Pathol 1982;137:177–180.
4. Kreipe H, Razdun HJ, Rudolph P, Barth J, Hansmann M, Heidorn K, Parwaresch MR. Multinucleated giant cells generated *in vitro:* Terminally-differentiated macrophages with down-regulated c-myc expression. Am J Pathol 1988;130:232–234.
5. Weinberg JB, Hobbs MM, Misukonis MA. Recombinant human gamma-interferon induces human monocyte polykaryon formation. Proc Natl Acad Sci USA 1984;81:454–457.
6. Hassan NF, Kamani N, Meszaros MM, Douglas SD. Induction of multi-nucleated giant cell formation from human blood-derived monocytes by phorbol myristate acetate in *in vitro* culture. J Immunol 1989;143:2179–2184.
7. Anderson JM. Implant retrieval and evaluation in biomaterials science: an introduction to materials in medicine. In: Ratner BD, Hoffman AS, Schoen FJ, Lemmons JE, editors. Biomaterials Science. New York: Academic Press; 1996. p 451–455.
8. Ziats NP, Miller KM, Anderson JM. In vitro and in vivo interactions of cells with biomaterials. Biomaterials 1988;9:5–13.
9. Zhao Q, Topham N, Anderson JM, Lodoen G, Payet CR. Foreign-body giant cells and polyurethane biostability: In vivo correlation of cell adhesion and surface cracking. J Biomed Mater Res 1991;25:177–183.
10. Anderson JM. Biological responses to materials. Annu Rev Mater Res 2001;31:81–110.
11. McInnis A, Rennick DM. Interleukin-4 induces cultured monocytes/macrophages to form multinucleated cells. J Exp Med 1988;167:598–611.
12. McNally AK, Anderson JM. Interleukin-4 induces foreign body giant cells from human monocytes/macrophages. Differential lymphokine regulation of macrophage fusion leads to morphological variants of multinucleated giant cells. Am J Pathol 1995; 147:1487–1499.
13. DeFife KM, Jenney CR, McNally AK, Anderson JM. Interleukin-13 induces human monocyte/macrophage fusion and macrophage mannose receptor expression. J Immunol 1997;158: 3385–3390.
14. Nakayama Y, Matsuda T. Surface macromolecular architectural designs using photo-graft copolymerization based on photochemistry of benzyl *N,N*-diethyldithiocarbamate. Macromolecules 1996;29:8622–8630.
15. DeFife KM, Colton E, Nakayama Y, Matsuda T, Anderson JM. Spatial regulation and surface chemistry control of monocyte/macrophage adhesion and foreign body giant cell formation by photochemically micropatterned surfaces. J Biomed Mater Res 1999;45:148–154.
16. Brodbeck WG, Shive MS, Colton E, Nakayama Y, Matsuda T, Anderson JM. Influence of biomaterial surface chemistry on apoptosis of adherent cells. J Biomed Mater Res 2001;55:661–668.
17. Marchant RE, Hiltner A, Hamlin C, Rabinovich A, Slobodkin R, Anderson JM. In vivo biocompatibility studies I. The cage implant system and a biodegradable hydrogel. J Biomed Mater Res 1983;17:301–325.
18. Spilezewski KL, Anderson JM, Schaap RN, Solomon DD. In vivo biocompatibility of catheter materials. Biomaterials 1988; 9:253–265.
19. Wu Y, Zhao Q, Anderson JM, Hiltner A, Lodoen G, Payet CR. Effect of some additives on the biostability of poly(etherurethane) elastomer. J Biomed Mater Res 1991;25:1415–1416.
20. Bergsma JE, Rozema FR, Bos RR, Boering G, de Bruijn WC, Pennings AJ. Biocompatibility study of as-polymerized poly(L-lactide) in rats using a cage implant system. J Biomed Mater Res 1995;29:173–179.
21. Suggs LJ, Shive MS, Garcia CA, Anderson JM, Mikos AG. In vitro cytotoxicity and in vivo biocompatibility of poly(propylene fumarate-*co*-ethylene glycol) hydrogels. J Biomed Mater Res 1999;46:22–32.
22. Brodbeck WG, Matsuda T, Jones JA, Colton E, Anderson JM. Biomaterial surface chemistry dictates adherent macrophage activation and cytokine mRNA expression. Transactions of the 27th Annual Meeting of the Society for Biomaterials, St. Paul, MN, April 24–29, 2001, p 214.
23. Jenney C, Anderson J. Adsorbed serum proteins responsible

for surface dependent human macrophage behavior. J Biomed Mater Res 2000;49:435–447.
24. Kao WJ, McNally AK, Hiltner A, Anderson JM. Role for interleukin-4 in foreign-body giant cell formation on a poly(ether-urethane urea) in vivo. J Biomed Mater Res 1995;29:1267–1275.
25. Chang JR, Zaczynska E, Katsetos CD, Platsoucas CD, Oleszak EL. Differential expression of TGF-b, IL-2, and other cytokines in the CNS of Theiler's murine encephalomyelitis virus-infected susceptible and resistant strains of mice. Virology 2000;278:346–360.
26. Zeyse D, Lunenfeld E, Beck M, Prinsloo I, Huleihel M. Interleukin-1 receptor antagonist is produced by sertoli cells in vitro. Endocrinology 2000;141:1521–1527.
27. Westphal J, Van't Hullenaar R, Peek R, Willems RW, Crickard K, Crickard U, Askaa J, Clemmensen I, Ruiter DJ, Waal DWRM. Angiogenic balance in human melanoma: expression of VEGF, bFGF, IL-8, PDGF and angiostatin in relation to vascular density of xenografts in vivo. Int J Cancer 2000;86:768–776.
28. Todt J, Sonestein J, Polak T, Seitzman GD, Hu B, Curtis JL. Repeated intratracheal challenge with particulate antigen modulates murine lung cytokines. J Immunol 2000;164:4037–4047.

Available online at www.sciencedirect.com
SCIENCE DIRECT®
Biomaterials 24 (2003) 4517–4527
Biomaterials
www.elsevier.com/locate/biomaterials

Phosphorylcholine-endcapped oligomer and block co-oligomer and surface biological reactivity

Takehisa Matsuda[a,*], Junichi Nagase[a,b], Akane Ghoda[a,b], Yoshiaki Hirano[b], Satoru Kidoaki[a,1], Yasuhide Nakayama[a]

[a] National Cardiovascular Center Research Institute, Department of Bioengineering, 5-7-1, Fujishiro-dai, Suita, Osaka 565-8565, Japan
[b] Department of Applied Chemistry, Osaka Institute of Technology, 5-16-1, Ohmiya, Asahi-ku, Osaka 535-0002, Japan

Abstract

Phosphorylcholine (PC)-endcapped oligomer and block co-oligomer were prepared by employing a photoiniferter-based quasi-living polymerization technique. The designed oligomer had a PC polar head group attached to an alkylene chain at one end of the molecule and an oligo(styrene) (oligoST) segment at the other end. In the co-oligomer, an oligo(*N*,*N*-dimethylacrylamide) (oligoDMAAm) segment was inserted between both ends of the oligomer mentioned above. Surface coating of these amphiphilic substances, using an appropriate coating procedure, resulted in a very hydrophilic characteristic, suggesting that the oligoST anchored on the substrate and the PC polar head group was exposed to or located on the outer coating layer. Non-cell adhesivity in serum-containing medium was observed, while slightly reduced protein adsorption was observed. Thus, PC-endcapped oligomer and block co-oligomer appear to function as a biocompatible coating.

Keywords: Phosphorylcholine; Block copolymer; Adsorption

1. Introduction

Biomembrane-mimetic surface designs with phosphorylcholine (PC) polar head group on blood- and tissue-contacting surfaces have been given great attention for possible biomedical applications. The logic behind this is based on the fact that the outer surfaces of living cell membranes have an assembly of PC-bearing lipids such as dipalmitoyl phosphatidylcholine, and that closely packed PC head groups in the cell membrane interact very mildly or minimally with proteins in blood or tissue fluid. Over 15 years, Chapman and colleagues [1–4,10] and Ishihara, Nakabayashi and colleagues [5–8] have conducted extensive studies to develop PC-bearing copolymers for blood-compatible surface coating.

In this study, we prepared an oligomer and a co-oligomer, both of which have a PC head group at one terminal end, as a biocompatible coating material. The strategy for synthesis is based on the utilization of the unique photochemistry of dithiocarbamate (an "iniferter" acting as initiator, transfer agent and terminator), which can dissociate into a radical pair upon ultraviolet (UV) irradiation and spontaneous recombination between them. This photochemistry has been extensively studied by Otsu and Yoshida [9] who pioneered the iniferter-based "quasi-living" photopolymerization of vinyl monomers in the early 1980s. This intrinsic characteristic of reversible photodissociation and recombination enable the preparation of well-controlled polymers and block copolymers in terms of chain length and block length [9].

As shown in Fig. 1, the designed PC-bearing oligomer and block co-oligomer molecules can be divided into three and four parts, respectively. A PC head group at one terminal end is attached to an alkylene chain. At the opposite terminal end, a water-insoluble styrene oligomer (oligoST) terminated with a dithiocarbamate group is installed to give α-phosphatidylcholine-ω-(*N*,*N*-diethyldithiocarbamyl)undecyl styrene oligomer. As for

*Corresponding author. Department of Biomedical Engineering, Graduate School of Medicine, Kyushu University, 3-1-1, Maidashi, Higashi-ku, Fukuoka 812-8582, Japan. Tel.: +81-92-642-6210; fax: 81-92-642-6212.
E-mail address: matsuda@med.kyushu-u.ac.jp (T. Matsuda).
[1] Present address: Department of Biomedical Engineering, Graduate School of Medicine, Kyushu University, 3-1-1, Maidashi, Higashi-ku, Fukuoka 812-8582, Japan.

0142-9612/03/$ - see front matter © 2003 Published by Elsevier Science Ltd.
doi:10.1016/S0142-9612(03)00344-2

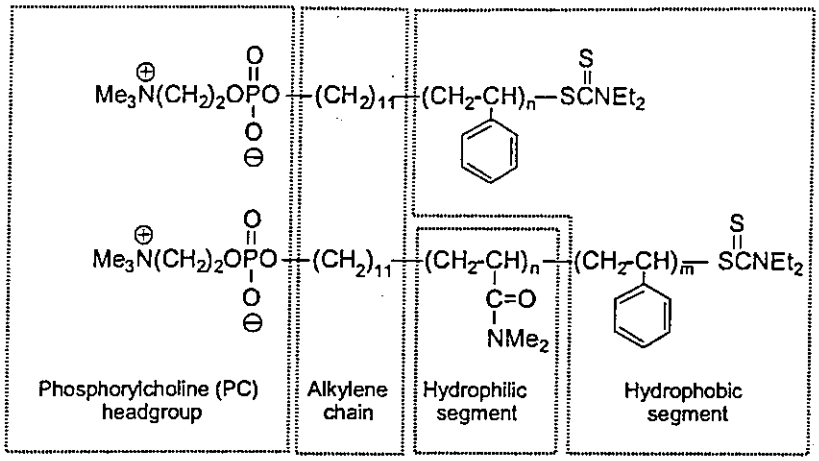

Fig. 1. Chemical structure of the designed PC-bearing oligomer and block co-oligomer.

the PC-bearing block co-oligomer, a water-soluble *N,N*-dimethylacrylamide oligomer (oligoDMAAm) was inserted in the center of the oligomer described above so as to combine the two ends of the oligomer to give α-phosphorylcholine-ω-(*N,N*-diethyldithiocarbamyl)undecyl oligoDMAAm–oligoST block co-oligomer. Surface characterization, protein adsorption and cell adhesion characteristics are discussed.

2. Experimental section

2.1. Materials

11-Bromo-1-undecanol, 2-chloro-2-oxo-1,3,2-dioxaphospholane and trimethylamine were obtained from Aldrich Chemical Co., Inc. (Milwaukee, WI, USA). Styrene (ST) was purchased from Ohken Co., Ltd. (Tokyo, Japan). 11-Mercapto-1-undecanol, which was synthesized as described in our previous studies [1,2], was kindly supplied by M. Hashimoto. Immunoglobulin G (IgG, human, fraction II) was purchased from United States Biochemical Corporation (Ohio, USA). Fibronectin was obtained from Koken Co., Ltd. (Tokyo, Japan). Albumin (bovine, fraction V) and dipalmitory phosphatidylcholine were obtained from Sigma Chemical Co. Ltd. (St. Louis, MO, USA). Poly(ethylene terephthalate) (PET) film for cell culturing, 1-dodecanethiol, solvents and other reagents, all of which are of special reagent grade, were obtained from Wako Pure Chemical Ind., Ltd. (Osaka, Japan).

2.2. Preparation of 11-(N,N-diethyldithiocarbamyl)-1-undecanol (1)

A solution of *N,N*-diethyldithiocarbamic acid sodium salt trihydrate (10.5 g, 47 mmol) in ethanol (70 ml) was placed in a 500 ml three-necked flask equipped with a stirrer, a dropping funnel and a reflux condenser. To this solution, 60 ml of an ethanolic solution of 11-bromo-1-undecanol (9.8 g, 39 mmol) was added dropwise at 50°C. After stirring for 8 h, the reaction mixture was filtered to remove sodium chloride, and then the filtrate was concentrated under reduced pressure. Then, the residue was poured into a large amount of water and extracted with ether. The organic phase was washed with water, dried (Na_2SO_4), filtered and evaporated under vacuum to yield 11.1 g of (1) as a white crystalline solid (91% yield). Analytically pure (1) was obtained by column chromatography on silica gel. Data for (1): ^{1}H NMR (DMSO-d_6 with Me_4Si) δ 3.96 (q, 2H, $J = 6.3$ Hz, $-CH_2$–N), δ 3.73 (q, 2H, $J = 7.2$ Hz, $-CH_2$–N), δ 3.40 (q, 2H, $J = 7.2$ Hz, $-CH_2$–OH), δ 3.19 (t, 2H, $J = 8.1$ Hz, $-CH_2$–S), δ 1.61 (tt, 2H, $J = 7.4$ Hz, CH_2–CH_2–S), δ 1.42–1.06 (m, 22H, CH_2–CH_2–CH_2, CH_2–CH_3); UV 279 (S=C–N), 252 (S=C–S).

2.3. Preparation of 11-(N,N-diethyldithiocarbamyl)undecyl phosphorylcholine (2)

A solution of (1) (4.8 g, 15 mmol) in acetonitrile (75 ml) was placed in a 200 ml glass pressure bottle. After cooling at −20°C, anhydrous trimethylamine (50 ml) in acetonitrile (50 ml) and 2-chloro-2-oxo-1,3,2-dioxaphospholane (7.7 g, 18 mmol) in acetonitrile (30 ml) were added to the solution. The pressure bottle was closed and heated at 60°C for 16 h. After standing at room temperature for 8 h, the reaction mixture was concentrated under reduced pressure. The resulting crude material was purified by column chromatography on silica gel to yield 2.2 g of (2) (30% yield). Data for (2): Rf = 0.1 (chloroform:methanol:water = 65:25:4); ^{1}H NMR (DMSO-d_6 with Me_4Si) δ 4.21 (br, 2H, $-CH_2$–O), δ 3.96 (q, 2H, $J = 7.2$ Hz, $-CH_2$–N), δ 3.79 (q, 2H, $J = 6.3$ Hz, $-CH_2$–N), δ 3.72 (t, 2H, $J = 5.4$ Hz, $-CH_2$–N), δ 3.63 (br, 2H, $-CH_2$–O), δ (t, 2H, $J = 8.1$ Hz,

$-CH_2-S$), δ 3.16 (s, 9H, N–CH_3) δ 1.50–1.63 (m, 4H, $-CH_2-CH_2-S$, $-CH_2-CH_2-O$), δ 1.14–1.12 (m, 20H, $CH_2-CH_2CH_2$, CH_3-CH_2); MS (EI) *m/e* (% relative intensity) 485 (100) M+, 368 (14), 307 (12), 184 (12), 154 (43), 136 (26) 116 (20).

2.4. Preparation of α-phosphorylcholine-ω-(N,N-diethyldithiocarbamyl)undecyl oligoST (3) and α-phosphorylcholine-ω-(N,N-diethyldithiocarbamyl) undecyl oligoDMAAm (4)

A mixture of (2) (12 mg, 0.025 mmol), DMAAm, (0.26 ml, 2.5 mmol) and tetraethylthiuram disulfide (7 mg, 0.025 mmol) in ethanol (4.74 ml) was placed in a 30 ml quartz tube. A stream of dry nitrogen was introduced through a gas inlet to sweep the tube for 5 min or more. The solution was then irradiated for 15 min using a 200 W Hg lamp (light intensity: 5 mW/cm^2, SPOT CURE, USHIO, Tokyo, Japan) in nitrogen atmosphere at 20–25°C. The reaction mixture was concentrated under reduced pressure. The residue was dissolved in a small amount of methanol. The precipitate, obtained by the addition of a large amount of ether, was separated by filtration. Reprecipitation was performed in the methanol–ether system. The last precipitate was dried in vacuum to yield 21 mg of (4) as a white powder. The molecular weight was 1100 g mol^{-1} (by GPC). As for PC-bearing oligoST (3), photoirradiation of a 20 ml mixture of (2) (0.05 g, 0.1 mmol) and ST (11.5 ml, 0.1 mol) in benzene for 15 min produced an oligomer (yield; 32 mg) with a molecular weight of approximately 1000 g mol^{-1}.

2.5. Preparation of α-phosphorylcholine-ω-(N,N-diethyldithiocarbamyl)undecyl oligoDMAAm–oligoST block co-oligomer (5)

A mixture of (4) (17 mg, 16 mmol) and ST (1.8 ml, 16 mmol) in a mixed solvent of benzene (1.6 ml) and methanol (1.6 ml) was photoirradiated similarly to the method above. Purification was performed by reprecipitation in the benzene–ether system to yield 30 mg of (5). The molecular weight was 2200 g mol^{-1} (by GPC).

2.6. Molecular characterization

All ^{1}H NMR spectra were recorded in DMSO-d_6 using tetramethylsilane (0 ppm) as an internal standard with a 270 MHz NMR spectrometer (GX-270, Tokyo, Japan) at room temperature. All Fourier transform infrared (FT-IR) spectra were measured using an FTIR-8200A spectrophotometer (Shimadzu, Kyoto, Japan) by the KBr method. Mass spectral analyses were performed in the Material Analysis Center of Osaka University (Osaka, Japan). UV absorption spectra were measured using a best-30 UV/VIS spectrophotometer (JASCO, Tokyo, Japan).

Number-average molecular weight (M_n) and weight-average molecular weight (M_w) were determined by gel permeation chromatography (GPC). The GPC equipment (HLC-8020 system, Tosoh, Tokyo, Japan) consisted of an RI detector and Tosoh TSKgel α3000 and α5000. Calibration was carried out using narrow-weight-distribution PEG standards (Tosoh), ranging from approximately 2×10^2–9.9×10^5 g mol^{-1}. The eluent used was *N,N*-dimethylformamide (DMF; HPLC grade) at a flow rate of 0.5 ml/min.

2.7. Surface coating of the co-oligomer

A benzene solution (50 μl) of (5) (0.5 wt%) was put on PET films (2.5 × 2.5 cm). After drying in air at room temperature, the treated films were rinsed with various solvents including chloroform, ethanol and 70% ethanolic solution.

2.8. Surface characterization

Advancing and receding contact angles toward deionized water were measured using a Kyowa contact angle meter (CA-D; Kyowa Kaimen Kagaku Co., Ltd., Tokyo, Japan) at 25°C using the sessile drop technique. At least five measurements were taken for each data point. Surface chemical compositions of the outermost layers were analyzed using an X-ray photoelectron spectrometer (XPS) (ESCA 750; Shimadzu Co., Kyoto, Japan). MgKα X-ray was used as the source. The photoelectron take-off angle was set at 15°. All binding energies were referenced to the carbon 1s component set to 285.0 eV. Overlapping peaks in XPS spectra were separated by a computer-aided curve-deconvolution method.

2.9. Surface plasmon resonance analysis

Surface plasmon resonance (SPR) analysis for IgG adsorption to the co-oligomer (5)-coated surface and to self-assembled monolayers (SAMs) of alkanethiolate as the control was carried out by the following procedure using a commercial SPR system (SPR670, Nippon Laser & Electronics Lab., Nagoya, Japan). A 5 μl droplet of 0.2% benzene solution of co-oligomer was placed and spread on gold-coated SPR sensor glass slides (Nippon Laser & Electronics Lab, Nagoya, Japan). After rinsing with ethanol, the glass slides were mounted in the SPR system. CH_3 group-packed and OH group-packed SAMs were prepared by immersion of the gold-plated glass slides into 1 mM ethanolic solution of 1-dodecanethiol or 11-mercapto-1-undecanol for 12 h and the glass slides were rinsed with ethanol. At first, phosphate-buffered saline (PBS; 137 mM NaCl, 2.68 mM KCl,

8.10 mM Na_2HPO_4, 1.47 mM KH_2PO_4, pH 7.4) was flushed over the co-oligomer (5)-coated surface or the SAM surface and a baseline for the SPR was maintained. IgG solution (100 μg/ml in PBS) was then allowed to flow through the system at a rate of 100 μl/min using a flow p ump. The adsorption process was monitored by the time-dependent change of SPR angle shift.

2.10. Cell attachment assay

Bovine endothelial cells (ECs harvested from the bovine aorta between the 10th and 14th passages) were used for cell adhesion test. The co-oligomer (5)-coated PET sheets, sterilized with 70% ethanol for 10 min and preincubated in PBS, were subjected to cell culture at a density of 2×10^4 cells/well (1.8 cm^2) and incubated in Dulbecco's modified Eagle's medium (DMEM; Flow Laboratories, McLean, VA, USA) supplemented with 10% fetal calf serum (FCS; purchased from Gibco Laboratories, Grand Island, NY, USA) at 37°C in a humid atmosphere of 95% air and 5% CO_2. After various incubation times, the morphology of the adhered cells was photographed using a phase-contrast microscope (DIAPHOT, Nikon, Tokyo, Japan) equipped with a Nikon camera (F3). The number of adhered ECs per unit area (0.25 mm^2) was determined from the phase-contrast microscopic images. Cell proliferation on the treated surface was expressed in terms of the number of attached cells per unit area.

3. Results

Fig. 2 shows sequential reactions leading to the preparation of PC-bearing block copolymers.

3.1. Preparation of phosphorylcholine-bearing iniferter (2)

The PC-bearing iniferter (2), 11-(*N*,*N*-diethyldithiocarbamyl)undecyl phosphorylcholine, was prepared as follows (Fig. 2): 11-(*N*,*N*-diethyldithiocarbamyl)-1-undecanol (1), prepared from 11-bromo-1-undecanol and sodium *N*,*N*-diethyldithiocarbamate (whose NMR spectra is shown in Fig. 3A), was reacted with 2-chloro-2-oxo-1,3,2-dioxaphospholane in the presence of trimethylamine [8,11]. The ^1H NMR spectrum (Fig. 3B) of the resultant product showed peaks of an *N*-methylene proton originating from the dithiocarbamyl group at 3.8 and 4.0 ppm. In addition, peaks of an *O*-methylene proton and an *N*-methyl proton, both of which originated from a PC group, were observed at 3.6 and 4.2 ppm, and at 3.2 ppm, respectively. The UV absorption spectrum (Fig. 4A) showed that absorption maxima equivalent to the S=C–S resonance system and the

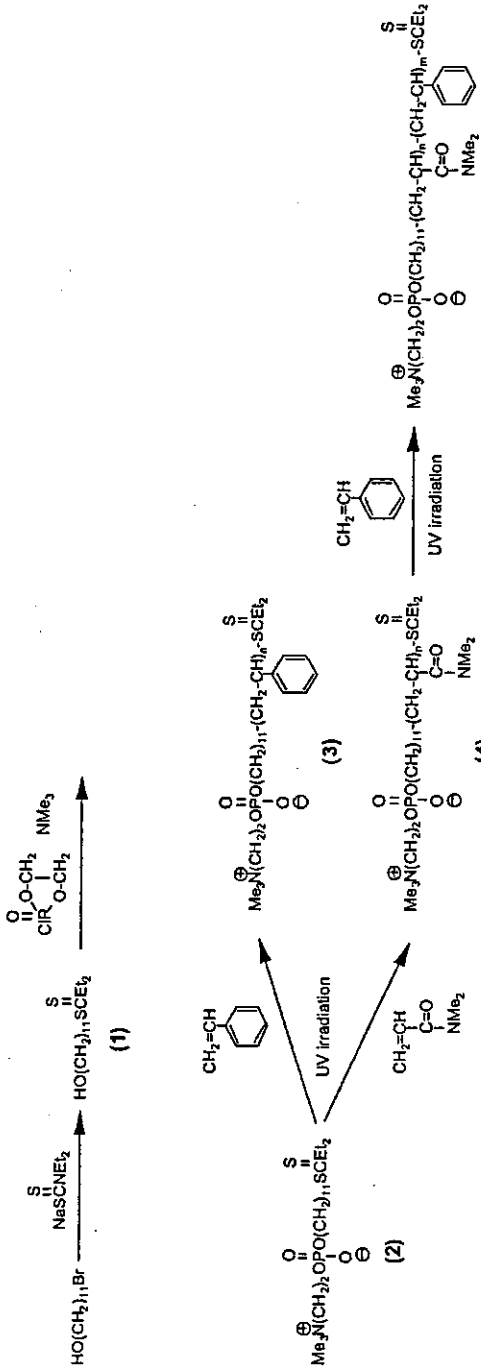

Fig. 2. Preparation scheme of phosphatidylcholine-endcapped oligomer (3) and co-oligomer (5): dithiocarbamylated phosphatidylcholine (2) was used as a photoiniferter. Upon UV irradiation in the presence of monomer (ST or DMAAm), a quasi-living polymerization proceeds to produce PC-bearing oligoST (3) or oligoDMAAm (4). PC-bearing co-oligomer (5) containing sequentially oligoST and oligoDMAAm was prepared by photopolymerization using iniferter-bearing oligoDMAAm (4) in the presence of ST monomer.

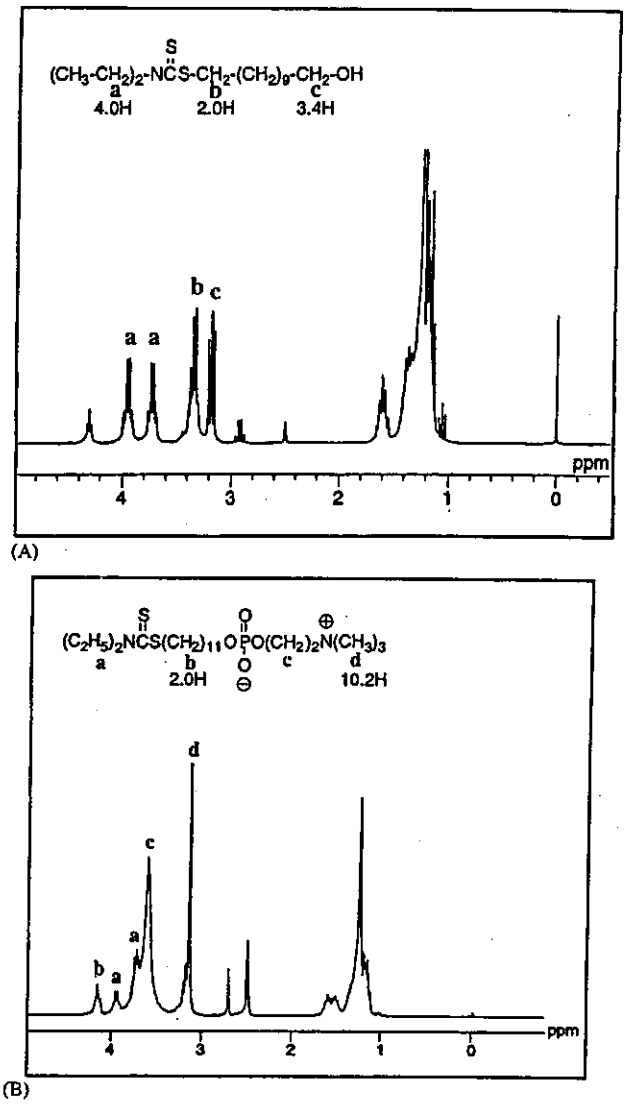

Fig. 3. ^{1}H NMR spectra of dithiocarbamyl derivative 1 (upper) and its phosphorylcholine derivative 2 (lower).

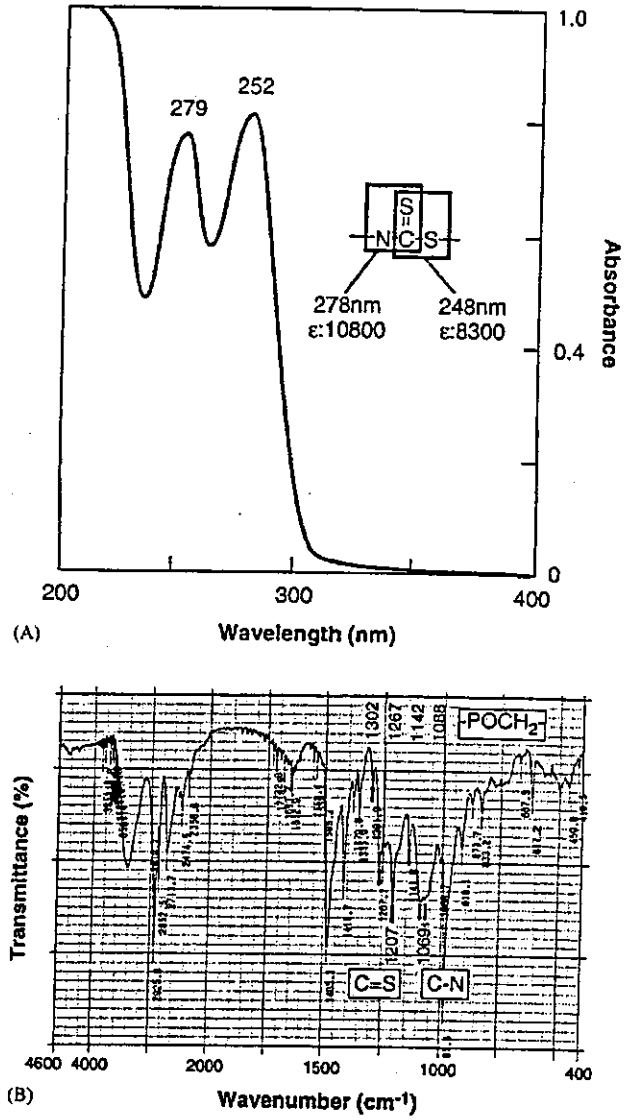

Fig. 4. UV spectrum (upper) and IR spectrum of the compound 2.

S=C–N one were observed at 252 and 279 nm, respectively. IR spectra shows the characteristic absorption peaks at 1207 cm^{-1} for C=S and 1069 cm^{-1} for C–N, and 1302, 1267, 1142 and 1088 cm^{-1} for CH_2 P=O (Fig. 4B). These indicate that PC-bearing iniferter (2) was synthesized.

3.2. Preparation of phosphorylcholine-endcapped oligoST (3) and oligoDMAAm–oligoST block co-oligomer (5)

The reaction scheme for the preparation of oligoST (3) and oligoDMAAm–oligoST block co-oligomer (5), both of which have a PC polar head group one end of the molecule, is shown in Fig. 2. PC-bearing oligoST (3) was prepared by the photoiniferter polymerization technique in the presence of ST. The quasi-living radical polymerization is described in the co-oligomer preparation as follows. In the case of co-oligomer (5), two-step photopolymerization was conducted. The first polymerization was initiated from PC-bearing iniferter (2) in an ethanolic solution of DMAAm under UV light irradiation to produce PC-endcapped oligoDMAAm. Subsequently, the second polymerization of ST was conducted in a mixed solution of benzene and methanol.

Fig. 5A shows the relationship between irradiation time and number-average molecular weight (M_n) in the polymerization of DMAAm from PC-bearing iniferter (2). An increase in UV irradiation time resulted in a linear increase in the molecular weight of the oligomer obtained. The degree of polydispersity (defined as the

ratio of weight-average to number-average molecular weight: M_w/M_n) remained at 1.2–1.3 during polymerization. The ^{1}H NMR spectrum showed that the obtained oligomer had a DMAAm unit (Fig. 6). The absorption maxima originating from a dithiocarbamyl group remained after UV irradiation. These indicate that the polymerization of DMAAm occurred via a quasi-living radical polymerization mechanism, resulting in the production of an oligoDMAAm segment having a PC group at one end and a dithiocarbamyl group at the other end. PC-bearing oligoDMAAm (4) with a molecular weight of approximately 1100 g mol^{-1} (approximately six units of DMAAm), which was obtained by 15-min irradiation in DMAAm solution, was subjected to irradiation in an ST-containing solution. As shown in Fig. 5B, M_n increased linearly with irradiation time, while the degree of polydispersities remained at approximately 1.3. The ^{1}H NMR spectra (Fig. 6) of the resulting product showed a peak of an aromatic ring originating from the ST unit at 7.1 ppm, while a peak of an *N*-methyl proton originating from the DMAAm unit remained near 2.9 ppm. Thus, the PC-bearing block co-oligomer (5) composing of oligoDMAAm and oligoST blocks was prepared.

Table 1 summarizes the composition of PC-bearing oligoST (3) and oligoDMAAm–oligoST block co-oligomer (5). The oligomer has a molecular weight of approximately 1000 g mol^{-1}, and the co-oligomer has a molecular weight of approximately 2200 g mol^{-1}, in

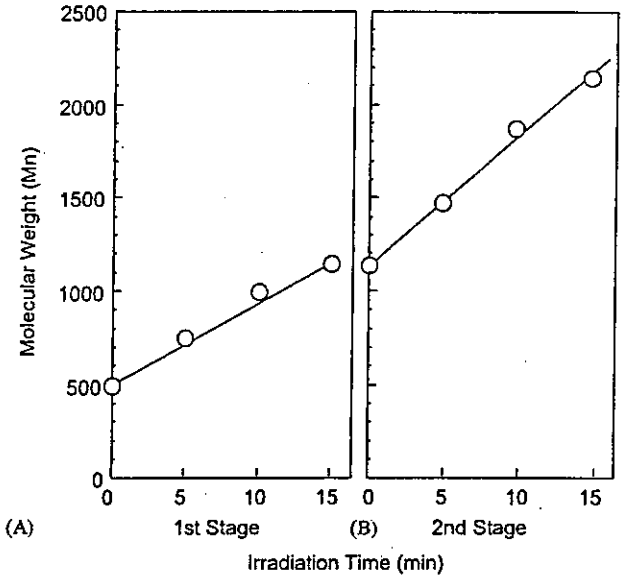

Fig. 5. (A) Photoirradiation time-dependent change in number-average molecular weight of oligoDMAAm (4) initiated from PC-bearing iniferter (2) and (B) change in number-average molecular weight of oligoDMAAm–oligoST (5) initiated from oligoDMAAm (4) (molecular weight: 1100 g mol^{-1}).

Table 1
Composition of PC-bearing oligoST (3) and oligoDMAAm–oligoST block co-oligomer (5)

Oligomer	M_n[a]	M_w of oligoDMAAm chain[b]	M_w of oligoST chain[b]
3	1000	0	500
5	2200	600 (6)	1100

[a] Determined by GPC measurements (calibrated with poly(ethylene glycol)).
[b] The molecular weights were calculated from the difference in M_n before and after photopolymerization.

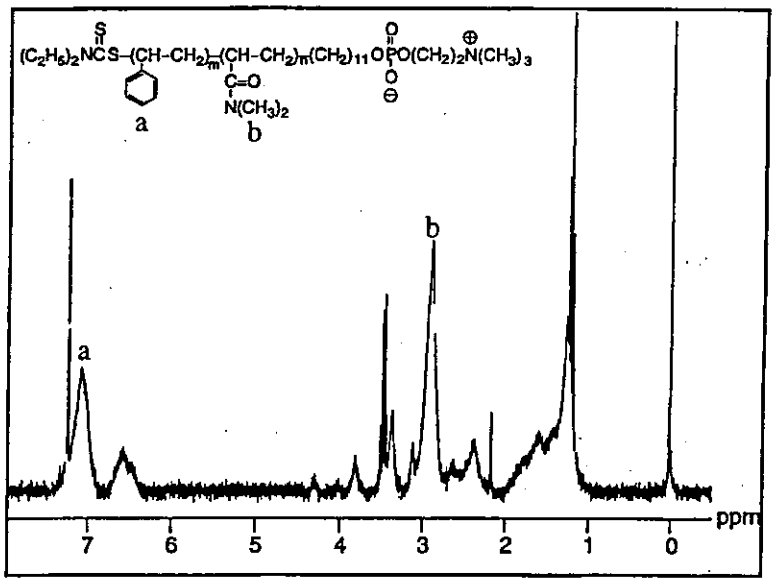

Fig. 6. ^{1}H MNR spectrum of the phosphorylcholine-bearing block co-oligomer of oligoST and oligoDMAAm.

which the oligoDMAAm segment has a molecular weight of approximately 600 g mol^{-1} and the oligoST segment approximately 1100 g mol^{-1} (note that each M_n of oligomer components was calculated from the difference in M_n before and after photopolymerization by GPC measurements). The compositional ratio of oligo ST and oligo DMAAm was identical to that determined from ^{1}H NMR spectra (Fig. 6). The co-oligomer has approximately six DMAAm units and 12 ST units in a molecule. The PC-bearing oligoST has an oligoST segment of approximately 500 g mol^{-1}. This indicates that the oligomer contains approximately five ST units in a molecule.

3.3. Surface coating of PC-bearing block co-oligomer

Fig. 7 shows the XPS spectra of oligomer (3)- and co-oligomer (5)-coated PET substrates: sulfur and phosphorus atoms were clearly detected for both oligomers. Upon rinsing with water, the advancing contact angle with water was 92° (which is almost the same as that of polystyrene) and the receding angle was 28° (Table 2). A phosphorus signal originating from the PC group was newly detected (P/C ratio; 1.3×10^{-3}). On the other hand, after rinsing with ethanol, benzene or chloroform, a small appreciable phosphorus signal in XPS spectra was observed. In contrast, as shown in Table 2, rinsing with 70% ethanolic solution of the coated film provided an advancing contact angle of 73°, a receding contact angle of 14° and an appreciable P/C ratio of 1.8×10^{-3}. These indicate that upon coating, the multilayered co-oligomer was formed on the PET surface (Fig. 8, (I)), which were difficult to remove by rinsing with water (II). However, the multilayered co-oligomer was eventually almost completely removed by rinsing with hydrophobic or polar solvents such as ethanol, benzene and chloroform (III). On the other hand, rinse with 70% ethanolic solution appeared to maintain the monolayer adsorbed directly on the PET film (IV). When the 70% ethanol-rinsed film was immersed in a 70% ethanol solution containing dipalmityl phosphatidylcholine (1 mg/ml), the P/C ratio was increased to 3.7×10^{-3} and water wettability was almost the same as that prior to phospholipid adsorption (Table 2), which is probably

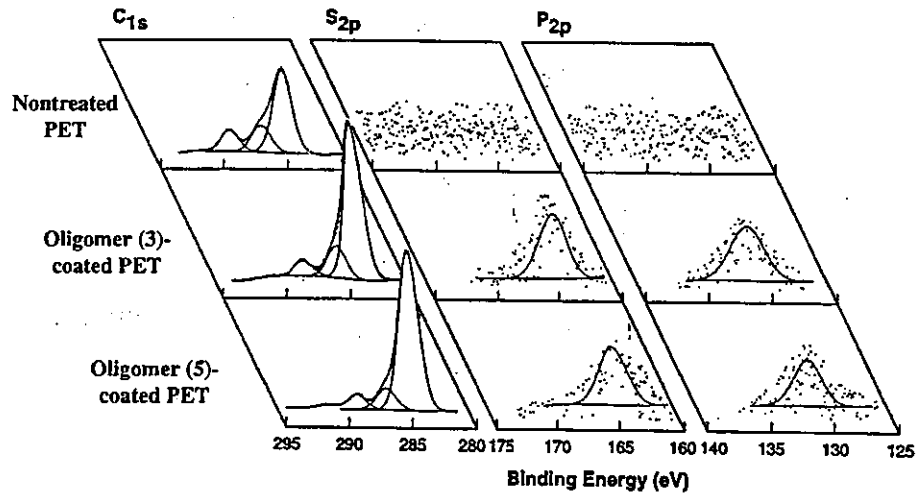

Fig. 7. XPS spectra (C_{1S}, S_{2P} and P_{2P} peaks) of non-treated PEG film, PC-bearing oligoST (3)-coated and PC-bearing oligoDMAAm–oligoST (5)-coated PET film surfaces.

Table 2
Surface chemical composition and water contact angles of (5)-coated PET film

Surface treatment		Solvent for rinsing	Water contact angle (deg)		P/C elemental ratio $\times 10^{-3}$
Coating with (5)	Post-adsorption of phosphatidylcholine		Advancing	Receding	
−	−		68	38	0
+	−	Water	92	28	1.3
+	−	Ethanol	62	30	0
+	−	Benzene	68	24	0
+	−	Chloroform	79	42	0
+	−	70% ethanol	73	14	1.8
+	+	70% ethanol	66	19	3.7